

1 Cas9 targeted nanopore sequencing with
2 enhanced variant calling improves
3 *CYP2D6-CYP2D7* hybrid allele genotyping

4 Rubben Kaat^{*,1} : kaat.rubben@ugent.be (KR)

5 Tilleman Laurentijn^{*,1} : laurentijn.tilleman@ugent.be (LT)

6 Deserranno Koen¹: koen.deserranno@ugent.be (KD)

7 Tytgat Olivier^{1,2}: olivier.tytgat@ugent.be (OT)

8 Deforce Dieter¹: dieter.deforce@ugent.be (DD)

9 Van Nieuwerburgh Filip^{1,†}: filip.vannieuwerburgh@ugent.be (FV)

10

11 *: equal contribution

12 ¹: Laboratory of Pharmaceutical Biotechnology, Ghent University,

13 Ottergemsesteenweg 460, 9000 Ghent, Belgium

14 ²: Department of Life Science Technologies, Imec,

15 Remisebosweg 1, 3001 Leuven, Belgium

16 [†]: Correspondence: filip.vannieuwerburgh@ugent.be

17 [Abstract](#)

18 *CYP2D6* is one of the most challenging pharmacogenes to genotype due to the high similarity with its
19 neighboring pseudogenes and the frequent occurrence of *CYP2D6-CYP2D7* hybrids. Unfortunately,
20 most current genotyping methods are therefore not able to correctly determine the complete *CYP2D6-*
21 *CYP2D7* sequence. Therefore, we developed a genotyping assay to generate complete allele-specific
22 consensus sequences of complex regions by optimizing the PCR-free nanopore Cas9-targeted
23 sequencing (nCATS) method combined with adaptive sequencing, and developing a new
24 comprehensive long read genotyping (CoLoRGen) pipeline. The CoLoRGen pipeline first generates
25 consensus sequences of both alleles and subsequently determines both large structural and small
26 variants to ultimately assign the correct star-alleles. In reference samples, our genotyping assay
27 confirms the presence of *CYP2D6-CYP2D7* large structural variants, single nucleotide variants (SNVs),
28 and small insertions and deletions (INDELS) that go undetected by most current assays. Moreover, our
29 results provide direct evidence that the *CYP2D6* genotype of the NA12878 DNA should be updated to
30 include the *CYP2D6-CYP2D7* *68 hybrid and several additional single nucleotide variants compared to
31 existing references. Ultimately, the nCATS-CoLoRGen genotyping assay additionally allows for more
32 accurate gene function predictions by enabling the possibility to detect and phase *de novo* mutations
33 in addition to known large structural and small variants.

34 [Author Summary](#)

35 During the last decades, the usefulness of personalized medicine has become increasingly apparent.
36 Directly linked to that is the need for accurate genotyping assays to determine the pharmacogenetic
37 profile of patients. Continuing research has led to the development of genotyping assays that perform
38 quite robustly. However, complex genes remain an issue when it comes to determining the complete
39 sequence correctly. An example of such a complex but very important pharmacogene is *CYP2D6*.
40 Therefore, we developed a genotyping assay in an attempt to generate complete allele-specific
41 consensus sequences of *CYP2D6*, by optimizing a targeted amplification-free long-read sequencing

42 method and developing a new analysis pipeline. In reference samples, we showed that our genotyping
43 assay performed accurately and confirmed the presence of variants that go undetected by most
44 current assays. However, the implementation of this assay in practice is still hampered as the selected
45 enrichment strategies inherently lead to a low percentage of on-target reads, resulting in low on-target
46 sequencing depths. Further optimization and validation of the assay is thus needed, but definitely
47 worth considering for follow-up research as we already demonstrated the added value for generating
48 more complete genotypes, which on its turn will result in more accurate gene function predictions.

49 [Introduction](#)

50 Genotyping is one of the most important aspects of personalized medicine, particularly within the
51 context of pharmacogenetics (1,2). In many medical disciplines, pharmacogenetic genotyping is used
52 to predict a patient's phenotype in order to adjust therapy (3,4). Especially the genetic variation in
53 drug-metabolizing enzymes significantly contributes to the differing benefit-risk balance of certain
54 drugs between patients (1,4). One of the essential drug-metabolizing enzymes is Cytochrome P450
55 2D6 (CYP2D6), as it is responsible for the metabolism or bioactivation of 20 to 30% of the clinically
56 used drugs (4). Therefore, accurate genotyping assays for this gene are of major importance. However,
57 although CYP2D6 is a relatively small gene spanning only 4400 nucleotides, accurate genotyping of this
58 gene is challenging. First of all, the CYP2D6 gene is surrounded by two pseudogenes showing 94%
59 sequence similarity with CYP2D6, which complicates the genotyping of this gene. Furthermore, CYP2D6
60 is one of the most polymorphic human genes, with over 100 star(*)-alleles and over 400 sub-alleles
61 (5,6). This star- and sub-allele nomenclature does not only encompass small sequence variations, such
62 as single nucleotide variants (SNVs) or insertions and deletions smaller than 50 bp (INDELs), but also
63 large structural variants, such as gene deletions and multiplications. On top of that, the possible
64 formation of hybrids with its nearest pseudogene CYP2D7 poses an additional major challenge when a
65 comprehensive genotype is desired (5–8).

66 In addition to the gene structure, a second important factor for accurate genotyping is the applied
67 genotyping assay. Various assays have been used for genotyping the *CYP2D6* gene, such as polymerase
68 chain reaction (PCR), microarrays, or short-read (SR) next-generation sequencing (NGS) (9–11).
69 However, most currently used assays target only a limited subset of pre-selected SNVs (12–14). Only a
70 few assays determine the correct genotype based on multiple detected SNVs and copy number
71 variations in each allele (13,15,16). Nevertheless, as 35.4% of the variant-drug interactions described
72 in the Clinical Annotations of PharmGKB are based on complete alleles containing all its variants, more
73 comprehensive genotyping assays could be valuable in the clinical practice (7,13,17). SR NGS
74 technologies can identify most individual variants in a genome, but mapping short reads to
75 homologous elements, such as those in *CYP2D6* and *CYP2D7*, is error-prone. On top of that, phasing of
76 short-read data is not straightforward, as it typically requires supplemental statistical phasing based
77 on known allele structures in the population or parental genotypic data (18).
78 Recently, efforts have been realized to comprehensively genotype *CYP2D6* in an attempt to overcome
79 these mapping and phasing problems (18–22). Different studies have shown that long-read sequencing
80 platforms can discover new variants and determine the correct allele structure (19,20). However, these
81 studies use long-range PCR to capture the targeted region, which is prone to template switching. This,
82 on its turn, results in chimeric PCR products and introduces phasing errors (23). To avoid the
83 application of long-range PCR (LR-PCR), a new enrichment strategy, called nanopore Cas9-targeted
84 sequencing (nCATS), was introduced by Gilpatrick *et al.* (24). This strategy uses targeted cleavage of
85 DNA with Cas9, followed by selectively ligating adapters for nanopore sequencing. However, ligation
86 of nanopore adapters to random breakage points also generates a considerable number of so-called
87 background reads, bringing the percentage of on-target reads down to merely 0.5% to 15% of the
88 sequenced reads in practice (24–26). To increase the number of reads on-target, a second PCR-free
89 enrichment strategy for nanopore sequencing, called adaptive sequencing (AS), could be used in
90 addition. AS refers to the ability of a nanopore sequencer to reject individual molecules in real-time

91 while they are being sequenced, and as such, does not involve additional steps in the library
92 preparation (27).

93 The aim of this study was to develop a new assay for correct and complete genotyping of complex
94 regions such as the *CYP2D6* gene. This genotyping assay consists of two important steps that need to
95 be optimized. The first step entails the generation of long reads using a PCR-free enrichment strategy
96 combined with nanopore sequencing. Therefore, the nCATS and combined nCATS-AS enrichment
97 strategies were both tested on the *CYP2D6-CYP2D7* locus. For this purpose, a guide RNA (gRNA) panel
98 was optimized to enrich *CYP2D6* and *CYP2D7* from human DNA samples. The second step aims to
99 correctly elucidate both large structural and small variants to determine the alleles of cell lines that
100 might contain both types of variants. However, the currently existing tools do not combine the
101 detection of large structural and small variants in one pipeline (28–31). Consequently, smaller variants
102 cannot be detected in regions with large structural variants, and large structural variants are not taken
103 into account when small variants are detected with currently available tools. This might lead to the
104 incorrect determination of gene sequences and complicate the correct assignment of star-alleles.
105 Therefore, we developed a new comprehensive long read genotyping (CoLoRGen) pipeline that is able
106 to simultaneously detect both large structural and small variants in complex genes such as *CYP2D6*.

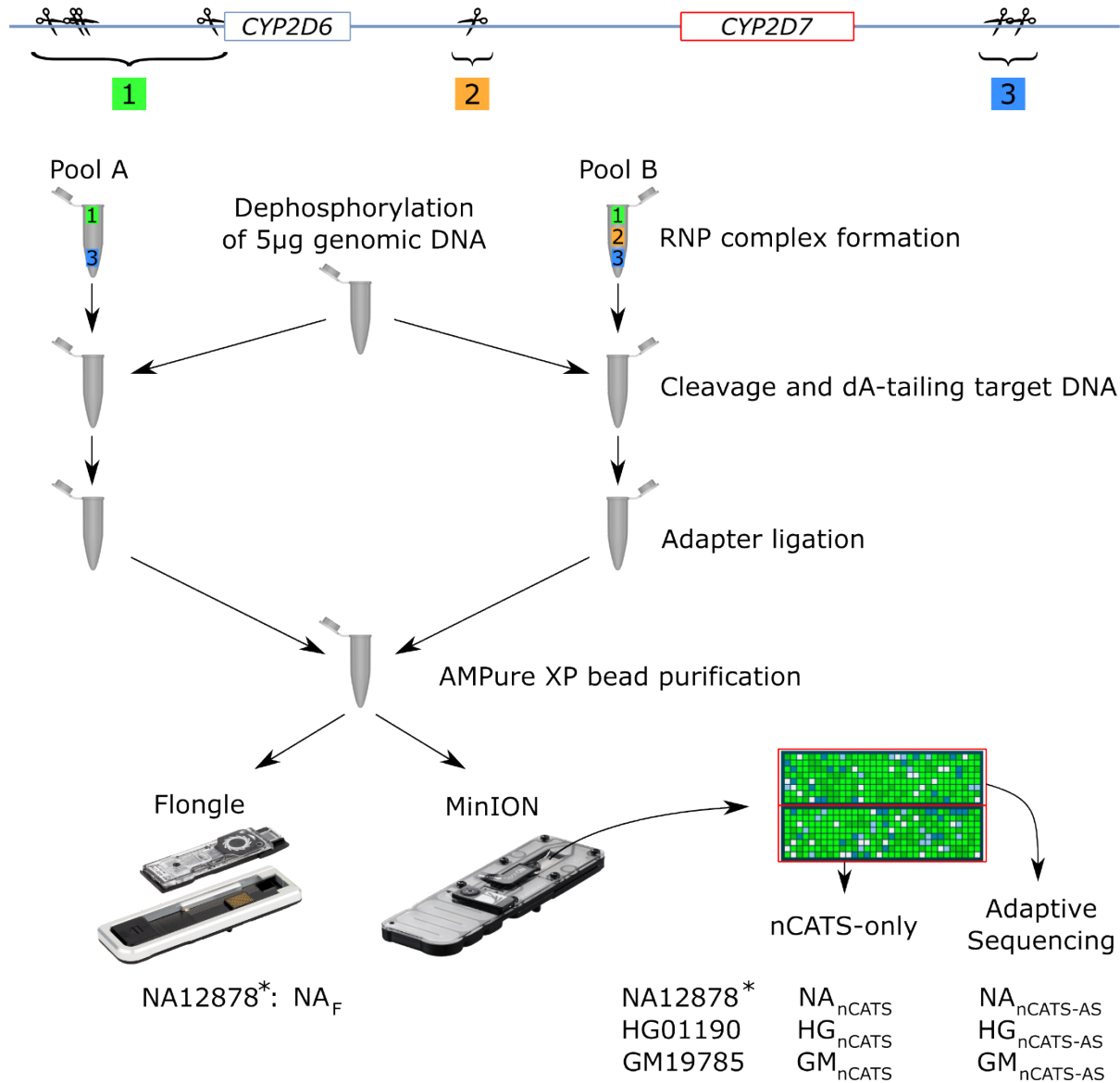
107 Materials and methods

108 Cell cultivation, DNA extraction, and nCATS

109 Two lymphoblast cell lines, HG01990 and GM19785, of which the *CYP2D6* genotype is well-known in
110 the literature (15,16), were cultivated and subsequently subjected to DNA extraction to obtain the
111 samples for the experiments conducted within this study. Cells were washed every three to four days
112 to an optimal cell density for successful cell growth of 300.000 cells/mL. The old medium was washed
113 away through 5-minute centrifugation at 500 to 600g, after which a new medium was added. The
114 medium contained 1% penicillin-streptomycin, 15% fetal bovine serum, and 2mM L-glutamine in
115 Roswell Park Memorial Institute (RPMI) 1640 medium. DNA samples were extracted using the DNeasy

116 Blood & Tissue kit (Qiagen, Venlo, The Netherlands), quantified using the Qubit fluorometer with the
117 dsDNA High Sensitivity Assay kit (ThermoFisher Scientific, Waltham, MA, USA), and stored at 4°C until
118 further processing. A Zymo DNA Clean & Concentrator purification step (Zymo Research, Irvine, CA,
119 USA) was performed to remove the excess salts, whereby the DNA was eluted in water. The length of
120 the eluted DNA fragments was measured on a Femto Pulse using the Agilent Genomic DNA 165 kb kit
121 (Agilent Technologies, Santa Clara, CA, USA) according to the manufacturer's recommendations.

122 The library preparation of the samples was performed according to the 'Cas9 targeted sequencing'
123 Oxford Nanopore Technologies (ONT) protocol, using the LSK-110 kit (ONT, Oxford, UK) (Figure 1). Nine
124 guide RNAs (gRNAs) were designed with the CHOPCHOP tool (32). Four of them were designed to cut
125 upstream *CYP2D6*, two downstream *CYP2D7*, and three between *CYP2D6* and *CYP2D7* (Table S1). The
126 gRNAs cutting between the two genes were added to ensure sufficient depth on *CYP2D6* for reliable
127 variant calling. The efficiency of the gRNAs was assessed beforehand in preliminary sequencing runs
128 using purchased NA12878 DNA. After selecting the seven most efficient gRNAs, two separate gRNA
129 pools were created. As shown in Figure 1, pool A only contained seven gRNAs that cut upstream
130 *CYP2D6* or downstream *CYP2D7*, whereas pool B also contained a gRNA that hybridizes between the
131 two genes. The use of two separate pools, one without gRNAs that cut between the genes, is necessary
132 to obtain reads covering the complete *CYP2D6*-*CYP2D7* locus. Active RNA ribonucleoprotein complex
133 (RNP) complexes were subsequently created in two separate tubes, using Alt-R® *S. pyogenes* HiFi Cas9
134 nuclease V3 (IDT, Leuven, Belgium), *S. pyogenes* Cas9 tracrRNA (IDT, Leuven, Belgium), and one of the
135 pools with *S. pyogenes* Cas9 Alt-R™ gRNAs (IDT, Leuven, Belgium).



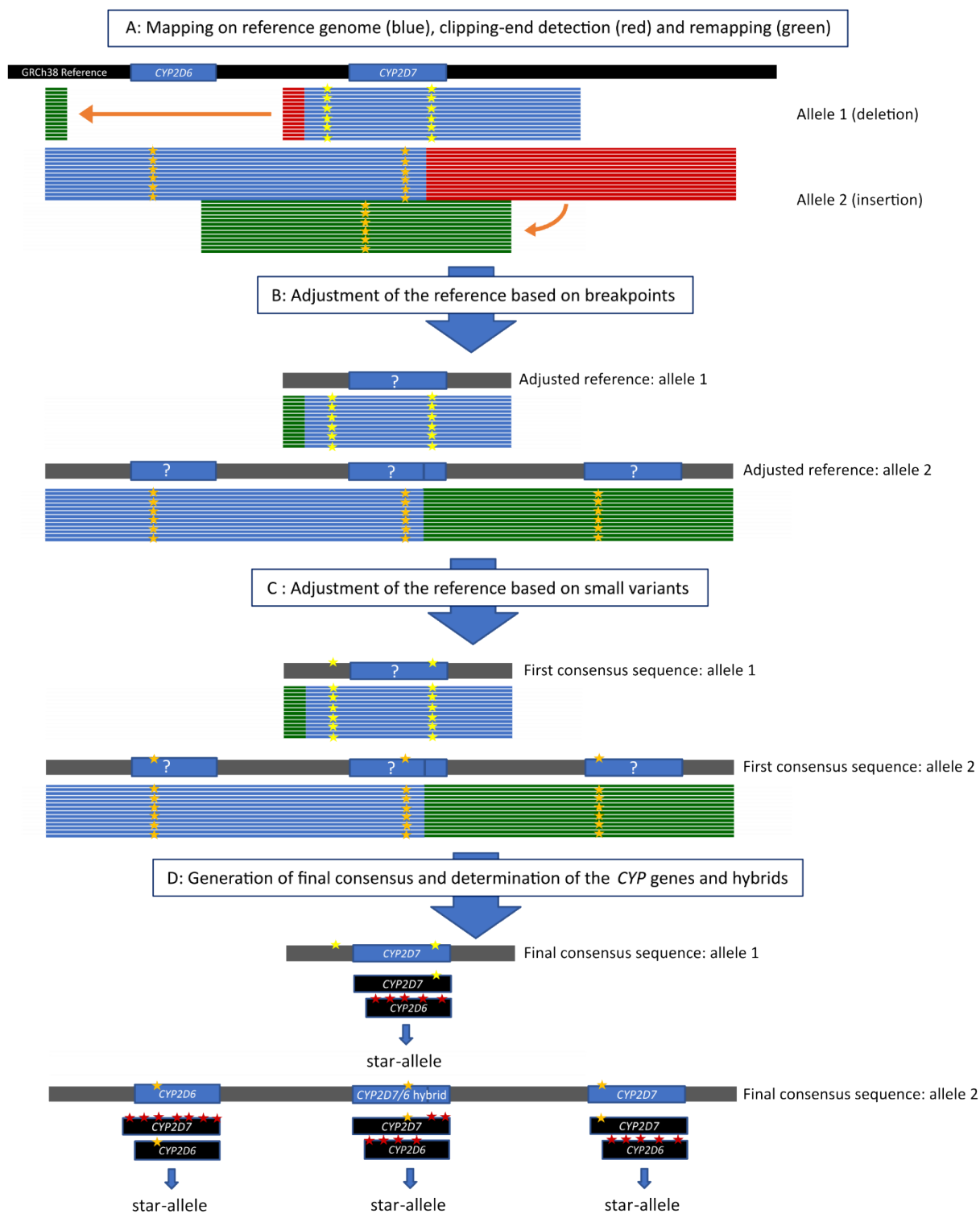
147 Five µg of purchased NA12878, extracted HG01990, and extracted GM19785 DNA was
148 dephosphorylated using Quick Calf Intestinal Phosphatase (NEB, Ipswich, MA, USA). The
149 dephosphorylated NA12878 DNA was added to one RNP complex pool with 9 and 8 gRNAs for the
150 MinION and Flongle library, respectively. The dephosphorylated DNA from the HG01990 and GM19785
151 cell lines was equally divided between the two Cas9 RNP complex pools. Subsequently, the target DNA
152 was cleaved by the active RNP complex, and Taq Polymerase (NEB, Ipswich, MA, USA) was added for
153 dA-tailing. Next, adapters were ligated to the newly produced DNA ends at the Cas9 cleavage sites by
154 adding 5 µL of Adapter mix II, 20 µL of Ligation Buffer, and 10 µL NEBNext Quick T4 DNA Ligase (NEB,
155 Ipswich, MA, USA) to the separate tubes. As the Cas9 enzyme remains bound to the DNA on the 5'-
156 side of the cleavage site, adapters are preferentially ligated on the 3'-side of the cleavage site. After
157 adapter ligation, the libraries were cleaned using a 0.3x volume of AMPure XP beads (Beckman Coulter,
158 High Wycombe, UK). First, 80 µL TE of pH 8 (IDT, Leuven, Belgium) was added to each tube. For the
159 HG01990 and GM19785 cell lines, the two separate tubes were pooled before adding the beads. 250
160 µL Long Fragment Buffer was subsequently used to wash the beads twice. After that, the beads were
161 resuspended in 10 and 14 µL Elution Buffer during a 30-minute incubation at room temperature for the
162 Flongle and MinION libraries, respectively. Before loading on a Flongle and MinION flow cell, 15 and
163 37.5 µL Sequencing Buffer, and 10 and 25.5 µL of Loading Beads were added to 5 and 12 µL of the
164 eluate, respectively. The DNA libraries were sequenced using an R9.4 Flongle or MinION flow cell on a
165 GridION device (ONT, Oxford, UK), and the AS software was activated on half of the pores of the
166 MinION flow cells. The flow cells ran up to 48h to obtain the maximum number of reads possible and
167 were controlled and monitored using the MinKNOW software.

168 Data analysis, variant calling, and star-allele assignment

169 The raw sequencing data was basecalled using the high accuracy model of Guppy (v5.0.7). Raw reads
170 were saved in fastq format, and only reads with a quality score above 8 were used for further analysis.
171 These reads were subsequently split up into two groups, based on whether they were generated by
172 pores controlled by the AS software or by pores that sequenced conventionally. All reads from the

173 latter group were used for further data analysis, whereas only the positively selected reads from the
174 first group were used in downstream analysis.

175 The data was processed with our in-house developed CoLoRGen pipeline to correctly assign both SNVs
176 and INDELs as well as large structural variants in the basecalled data. To detect all these variants at
177 once, several consecutive steps were carried out by the CoLoRGen pipeline (Figure 2). First, the reads
178 were mapped against the human GRCh38 reference genome using Minimap (v2.18) (Figure 2A). Only
179 the reads that mapped on the target region were retained for further analysis. Variant calling was
180 performed on these reads using the Medaka Variant pipeline (v1.4.3). Based on the called SNVs and
181 INDELs, the reads were split into two alleles using WhatsHap (v1.1). Breakpoints of large structural
182 variants were defined for each allele separately, based on the starting points of clipping ends and the
183 mapping coordinates of these clipping ends when mapped separately (red and green reads in Figure
184 2A, respectively). Only breakpoints covered by at least three reads were considered in order to obtain
185 accurate structural variant calling. In the next step, an adjusted GRCh38 reference genome was built
186 for each allele (Figure 2B). This adjusted reference contained the large structural variants of the DNA
187 under study, based on the defined breakpoints. Then, the reads from both alleles were mapped once
188 again, this time against the corresponding self-constructed and more representative reference
189 sequence for each allele. After that, a first consensus sequence for each allele was deduced using the
190 Medaka Consensus pipeline (v1.4.3) (Figure 2C). Subsequently, the consensus sequences for the two
191 alleles were further optimized by mapping all the initially mapped reads to the GRCh38 target region.
192 Reads that did not map unambiguously on one of the alleles were removed from the mapping data.
193 Based on the newly mapped reads, the consensus sequences were finalized, and an accompanying
194 probability file was generated using the Medaka Consensus pipeline (v1.4.3) (Figure 2D).



195

196 *Figure 2* Workflow of the in-house developed CoLoRGen pipeline, which combines large structural and small variant calling.

197 A: The basecalled reads are mapped against the human reference genome GRCh38 (black). Reads are split into the two alleles

198 based on the small variants (yellow and orange stars). Clipping ends of the reads (red) are cut in-silico and mapped again to

199 the reference genome (green). B: The reference is adapted based on the breakpoints of the clipping ends in the DNA under

200 study (grey). Reads of alleles 1 and 2 are mapped against their respective adjusted reference sequence to create a first

201 consensus sequence. C: The reference sequences are further adjusted by mapping all the previously mapped reads to end up
202 with a final consensus sequence. D: The GRCh38 sequences of the *CYP2D6* and *CYP2D7* genes are mapped against the final
203 consensus sequences. The GRCh38 gene or fragment containing the least mismatches (red stars) is assigned to the
204 corresponding gene or fragment of the consensus sequence, resulting in the determination of the corresponding genes and
205 hybrids. Finally, star-alleles can be assigned based on the determined variants.

206 Finally, the genes or hybrids in the consensus sequence were exactly identified based on their small
207 variants (Figure 2D). For this purpose, the GRCh38 references of the *CYP2D6* and *CYP2D7* genes were
208 mapped to the final consensus sequence of each allele, and mismatches between the consensus and
209 the GRCh38 references were called using the Medaka Variant software (v1.4.3). The GRCh38 gene or
210 fragment containing the least mismatches was assigned to the corresponding gene or fragment in the
211 consensus sequence. Hybrids of *CYP2D6* and *CYP2D7* were reconstructed by concatenating these
212 generated fragments, and a quality score was assigned to each small variant by considering the
213 probability distribution on that exact position. By completing these steps, the number of copies of each
214 gene and the exact composition of the hybrids were determined for each allele. After that, the star-
215 alleles defined in PharmVar were assigned to the consensus alleles using a look-up algorithm based on
216 the variants present in each gene (33). The star-allele or sub-allele most similar in terms of variants
217 was assigned to the alleles of each sample.

218 The newly developed CoLoRGen pipeline was benchmarked using the NA12878 hybrid Genome in a
219 Bottle Consortium (GIAB)-Platinum Genomes benchmark dataset described by Krushe *et al.* (34). VCF-
220 files for the *CYP2D6* and *CYP2D7* genes of our data were separately compared with the benchmark
221 dataset using the hap.py software (35). Visualizing the variants and verifying if they were correctly
222 called and phased was done with in-house developed python scripts (36).

223 The sequencing data from the MinION run with NA12878 DNA was subsampled to determine the 16X
224 minimum depth needed for reliable detection of small variants. Subsampling of the raw data was
225 carried out using Seqtk (37). The CoLoRGen pipeline was run on each subsample. For each subsample,
226 the depth of both genes was calculated, and the number of false- and true-positives was determined

227 using in-house developed python scripts. In the subsampled datasets with depths below 16X on a gene,
228 more than one false-positive variant popped up compared to the complete dataset. Therefore, a
229 minimum depth of 16X on each allele of each gene was set as the lower limit for reliable small variant
230 detection.

231 The CoLoRGen pipeline and the additional scripts are available via GitHub and can also be used for
232 other genes when adapting the target gene regions and adding correct references for the star-alleles
233 (36,38).

234 Results and discussion

235 Optimization of the nCATS experimental set-up

236 The *CYP2D6-CYP2D7* locus from the CEPH/UTAH pedigree 1463 sample NA12878 was first sequenced
237 on a MinION flow cell to evaluate the cleavage and enrichment efficiency of the designed gRNAs, and
238 to assess their off-target binding potential. Visualizing the mapped reads showed an additional
239 cleavage place to the ones that were expected for the designed gRNAs. This additional cleavage place
240 was due to off-target binding and cleavage of the RNP with gRNA9 (Figure S1). Therefore, gRNA9 was
241 omitted in the subsequent sequencing runs. The eight remaining gRNAs were used to prepare a
242 NA12878 Flongle library (NA_F) to confirm the previous results. However, the selection of gRNAs still
243 proved to be suboptimal, as the reads revealed the generation of smaller fragments. This was due to
244 the high cleavage efficiency of the RNP with gRNA3, which as a result, created smaller fragments
245 instead of increasing the depth on-target (Figure S2). Hence, gRNA3 was omitted in the subsequent
246 sequencing runs as well. Furthermore, as almost no reads covering the complete *CYP2D6-CYP2D7* locus
247 were present in the data from these preliminary sequencing runs, two pools with gRNAs were created
248 for the subsequent runs. One pool did not contain the gRNA that cleaves between *CYP2D6* and *CYP2D7*
249 to increase the number of reads covering the complete locus in the subsequent datasets.

250 Enrichment of the *CYP2D6-CYP2D7* locus using nCATS or nCATS-AS

251 The enrichment efficiencies of both the nCATS-AS and the nCATS-only enrichment strategies were

252 assessed during this study. For this purpose, the abovementioned nCATS enriched NA12878 library

253 was sequenced on a MinION flowcell of which half of the pores were controlled by the AS software

254 (NA_{nCATS-AS}), and the other half of the pores were sequenced conventionally (NA_{nCATS}). The NA_{nCATS-AS}

255 data obtained an on-target depth of 128X, which was a 1.16 times increase compared to the NA_{nCATS}

256 data (Table 1). After the preliminary sequencing runs with NA12878 libraries, two additional MinION

257 runs were performed on libraries from extracted HG01990 (HG_{nCATS-AS} and HG_{nCATS}) and GM19875

258 (GM_{nCATS-AS} and GM_{nCATS}) DNA. The purpose of these runs was to evaluate if the enrichment strategies

259 can generate correct *CYP2D6* and *CYP2D7* alleles for cell lines containing large structural variants. For

260 these libraries, the two separate pools with the final selection of gRNAs were used. Furthermore, the

261 same AS conditions as for the first MinION run were applied to additionally determine if AS exhibits

262 added value for the enrichment of the *CYP2D6-CYP2D7* locus in these cell lines. The HG_{nCATS-AS} and

263 HG_{nCATS} libraries reached an on-target depth of 25X and 30 X, respectively. Lower depths of 7X and 12X

264 were obtained for the GM_{nCATS-AS} and GM_{nCATS}, respectively (Table 1).

265 *Table 1* General sequencing results of the nCATS-enriched NA12878, HG01990, and GM19785 libraries.

	NA12878			HG01990			GM19785		
	nCATS-AS	nCATS	Combined	nCATS-AS	nCATS	Combined	nCATS-AS	nCATS	Combined
Throughput (MB)	500	5 000	5,500	7	92	99	0.7	138	139
Total reads	588,959	2,213,701	2,802,660	1,470	11,066	12,536	771	18,778	19,549
Reads on-target	935	806	1,741	131	146	277	43	69	112
Average target depth	128X	110X	238X	25X	30X	55X	7X	12X	19X
Percentage on-target (%)	0.16*	0.04*	0.06	8.91	1.32	2.21	5.58	0.37	0.57

266 Each library was sequenced on one flow cell with half of the pores in AS mode, and half of the pores in uncontrolled mode.

267 ‘nCATS-AS’ refers to the data of the pores in AS mode; ‘nCATS’ refers to the data generated by the uncontrolled,

268 conventionally sequencing pores; ‘combined’ (values in bold) refers to the combined dataset containing both the positively

269 selected reads from the AS pores and all the reads from the conventionally sequencing pores. *: In this run, multiple *CYP*-

270 genes were enriched with separate gRNA pools. Therefore, these on-target percentages should not be compared with the

271 on-target percentages of the other runs.

272 The use of the AS software in addition to the nCATS enrichment did not consistently result in a higher

273 on-target depth, but it did result in a considerably higher on-target percentage for all three cell lines

274 (Table 1). However, as the vast majority of the strands were rejected by the software, the throughput

275 generated by the AS controlled pores was also proportionally lower. Moreover, there were no more

276 target strands encountered in the adaptive sequencing pores, as the rejected DNA strands were not

277 removed from the flow cell, thus still hindering the accessibility of the pores. Overall, this resulted in

278 approximately the same absolute number of on-target reads compared to the other pores, for which

279 only nCATS-enrichment was used. Therefore, it can be concluded that the AS software does not

280 conclusively offer sufficient additional benefit in this context. However, the advantages of adaptively

281 sequencing certain specific strands have already been demonstrated in other contexts (27,39).

282 The enrichment efficiency of the nCATS strategy on itself was assessed as well. In their Cas9 targeted

283 sequencing protocol, ONT mentions that a minimum target depth of 100X should be achievable (40).

284 This depth was only obtained for the first MinION run in this study. All other runs reached a combined

285 target depth of the AS-controlled and conventionally sequencing pores below 60X (Table 1). This value

286 is expected to be influenced by two important factors that should be considered when determining

287 the nCATS experimental set-up. The first factor is the number of gRNAs used for each target. ONT

288 recommends using four gRNAs for regions smaller than 20 kb, two upstream of the target region and

289 two downstream. Adding additional gRNAs at one side of the target region increases redundancy, so

290 there is always at least one properly functioning gRNA in case of mutations in the recognition site of

291 one of the other gRNAs at that position (26). As four gRNAs were designed upstream of *CYP2D6* and

292 two downstream of *CYP2D7* in this study, this factor can be eliminated as a possible issue. The second

293 factor to consider is the length of the input DNA. When the target region is longer than the average
294 length of the input DNA, the depth drops towards the center part of the targeted region. Moreover,
295 the target length increases when gene insertions or duplications are present, thereby complicating the
296 achievement of sufficient depth even more. To increase the depth in the center of the targeted region,
297 ONT advice is to follow the tiling approach, as described in their protocol (40). In the tiling approach,
298 two pools of gRNAs are used. Each pool generates fragments that overlap with the fragments of the
299 other pool. However, the downside of using the tiling approach is that fewer or no full-length reads of
300 the gene construct are generated. To overcome this drawback, two different gRNA pools were
301 composed in this study, one containing gRNAs that cut upstream and downstream the *CYP2D6-CYP2D7*
302 locus, and another one also containing a gRNA cutting the DNA between the two genes. The input DNA
303 was divided into two tubes, and each tube was incubated with a different gRNA pool to obtain reads
304 covering the full *CYP2D6-CYP2D7* locus but also enrich the depth in the middle of the locus. Moreover,
305 using a gRNA that cuts in the middle of the locus also aids in obtaining sufficient depth on *CYP2D6* for
306 reliable variant calling. However, although these two factors were considered for our experimental
307 set-up, the predetermined target depth was not obtained in this study.

308 Another factor influencing the obtained target depth is the percentage of on-target reads. PCR-free
309 enrichment using nCATS generally resulted in a low percentage of on-target reads. Even after
310 optimizing our customized pools of gRNAs for the *CYP2D6-CYP2D7* locus, a maximum on-target
311 percentage of only 1.32% could be reached when this enrichment method was used without AS (Table
312 1). ONT reference samples comparable in length achieve an on-target percentage of 0.4% (26).
313 Although our results are better, the obtained enrichment remains limited. Background DNA is assumed
314 to be the main cause for this limited enrichment, as the number of off-target reads was only about 1%.
315 The large amount of sequencable background DNA is probably due to the inefficiency of certain
316 protocol steps or breakage of DNA strands when handling the DNA, making phosphorylated ends to
317 which an adaptor can bind. Besides carefully executing the steps of the protocol, no other
318 measurements could have been implemented to increase this percentage. Logically, this low obtained

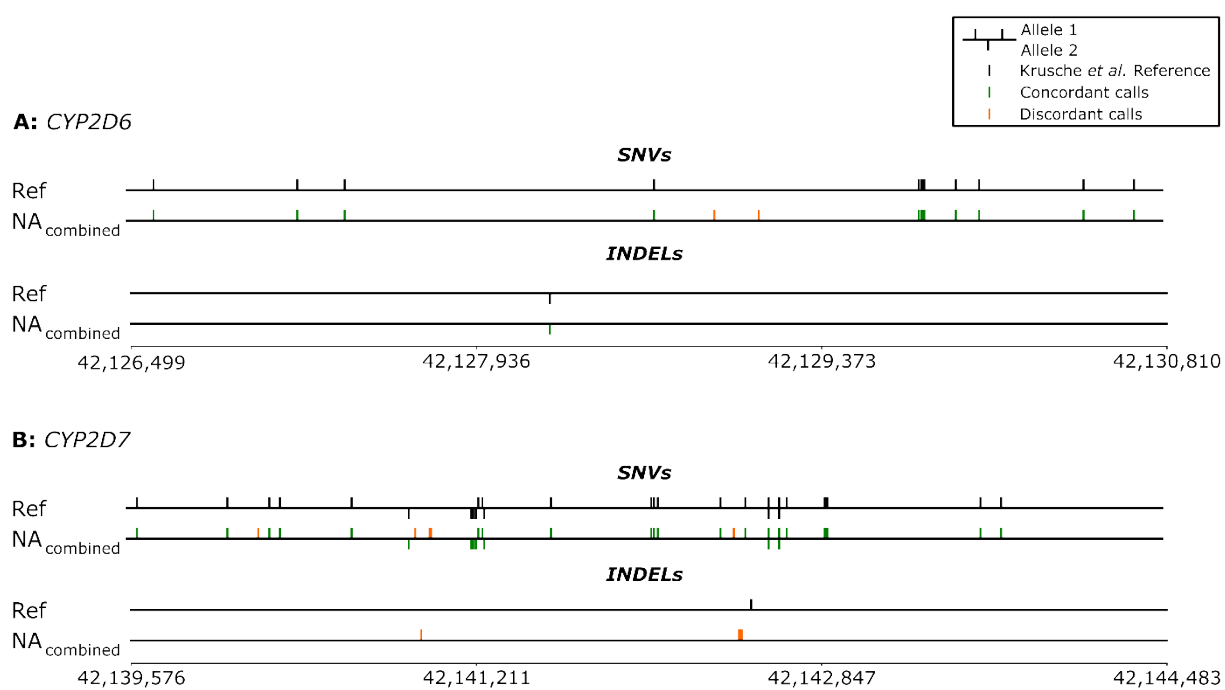
319 percentage of on-target reads on its turn resulted in a low depth on target. However, this is not the
320 only factor inherent to the nCATS protocol that influences the maximum obtainable target depth.

321 The overall throughput of the sequencing run also plays an important role in obtaining sufficient target
322 depth. The nCATS protocol generated low throughputs for all three DNA samples (Table 1). This is
323 caused by the presence of non-adaptor-ligated DNA strands in the flow cell, as these are not removed
324 during the library preparation. These DNA strands are assumed to spatially block the pores, thereby
325 hindering the sequencing of the adaptor-ligated DNA strands and causing a very low pore occupancy.
326 The low target depth ensuing from the background and non-adaptor-ligated DNA strands comprises
327 one of the main disadvantages of the nCATS enrichment method in the pharmacogenetics context. It
328 implies that one flow cell per patient is needed to get enough depth on the targeted region(s), resulting
329 in a high sequencing cost that hinders the implementation of the proposed assay in practice.
330 Optimizing the nCATS protocol by incorporating an additional purification step for the adaptor-ligated
331 strands might solve this issue and increase the on-target depth, allowing multiple samples to be
332 sequenced on one flow cell. The establishment of a purification step compatible with the nCATS-
333 protocol constitutes the follow-up research to this paper.

334 SNV and INDEL calling performance on reference NA12878 DNA

335 The small variant calling performance of the nCATS enrichment strategy combined with the CoLoRGen
336 analysis pipeline was assessed using the NA12878 library, as only for this DNA a truth set containing all
337 small variants is available in the literature (34). For this purpose, the NA_{combined} dataset was used,
338 combining the nCATS-AS and the nCATS reads, as the only difference between these reads is the
339 specific pore on the same flow cell it was sequenced on. The truth set composed by Krusche *et al.* (34)
340 contains 11 SNVs and 1 INDEL in the *CYP2D6* gene, and 26 SNVs and 1 INDEL in the *CYP2D7* gene (Figure
341 3). All 11 and 26 SNVs in *CYP2D6* and *CYP2D7*, respectively, were also called and phased in the NA_{combined}
342 dataset (Figure 3). However, two additional, supposedly false-positive SNVs were called in *CYP2D6*,
343 and five in *CYP2D7*. As for the INDELs, only the deletion in *CYP2D6* was called and phased correctly.

344 The insertion in *CYP2D7* remained undetected, but four additional deletions were detected in the
345 $\text{NA}_{\text{combined}}$ consensus of *CYP2D7* instead. Remarkably, all supposedly false-positive SNVs and INDELs in
346 both genes were assigned to the same allele after phasing. This raises the question as to whether the
347 NA_{12878} reference by Krusche *et al.* is incorrect, and consequently the false-positive variants are
348 actually present in the NA_{12878} DNA. Additional results and discussions on this can be found in the
349 sections below.

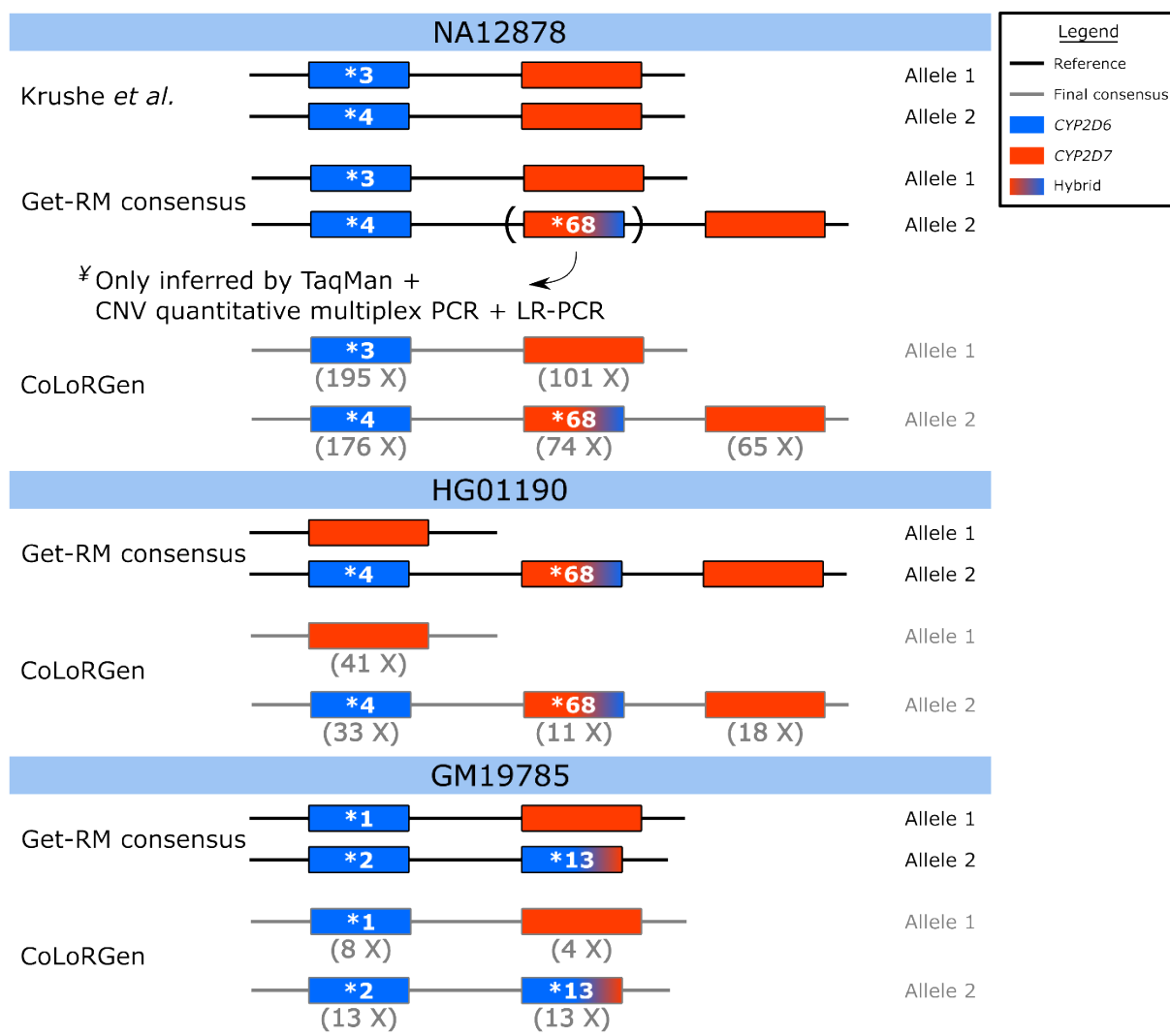


350
351 *Figure 3* Representation of the called and phased small variants (SNVs and INDELs) in the *CYP2D6* and *CYP2D7* genes of the
352 $\text{NA}_{\text{combined}}$ library. The truth set composed by Krusche *et al.* (34) was used as reference (Ref). Green lines represent concordant
353 calls (true-positives compared to the truth set), which are correctly called and phased variants compared to the reference;
354 orange lines represent discordant calls (false-positives compared to the truth set). Note: multiple variants next to each other
355 are visually represented by thicker lines.

356 Comprehensive genotyping of the NA_{12878} *CYP2D6*-*CYP2D7* locus by the CoLoRGen
357 pipeline

358 The CoLoRGen pipeline detected a structural variant in addition to the small variants in the NA_{12878}
359 DNA. Based on all the detected variants, CoLoRGen assigned the *CYP2D6* *3/*4+*68 star-alleles to the
360 $\text{NA}_{\text{combined}}$ dataset, of which the *68 allele represents a *CYP2D6*-*CYP2D7* hybrid insertion (Figure 4). The

361 high obtained on-target depth of 238X implicates that the detection of this hybrid cannot be attributed
362 to nanopore sequencing errors or an artifact of the analysis pipeline. However, no large structural
363 variants have been identified for the *CYP2D6-CYP2D7* locus in the NA12878 hybrid benchmark of
364 Krusche *et al.* (34). Accordingly, the Get-RM studies did not unambiguously assign a structural variant
365 to the NA12878 DNA (15,16). In these Get-RM studies, several testing laboratories conducted different
366 assays, but only when TaqMan-based genotyping was combined with CNV and structural variant
367 detection using quantitative multiplex PCR and LR-PCR validation, the presence of the *68 hybrid could
368 be detected (15). Therefore, the *68 allele was not included with 100% certainty in the reported
369 consensus star-allele classification (15). In accordance with our results, a more recently published
370 article also reported the statistical inference of the *68 allele in NA12878 whole-genome sequencing
371 (WGS) data when using the Cyrius analysis tool (41). As the *68 hybrid has been inferred in the
372 NA12878 DNA multiple times in literature, it can be concluded that this structural variant is effectively
373 present and was thus correctly identified by the CoLoRGen pipeline.



375 *Figure 4* Star-alleles in literature references and star-alleles assigned by the CoLoRGen pipeline. Reference star-alleles were
376 obtained from Krushe *et al.* (34) and the Get-RM studies (15,16). The depths mentioned below the genes are the generated
377 average depths on that position of the locus. *The *68 allele was only detected when TaqMan-based genotyping was
378 combined with CNV and structural variant detection using quantitative multiplex PCR and LR-PCR validation. Therefore, the
379 Get-RM consensus star-allele only mentions the *68 allele in brackets. Note: even when depths below the minimal 16X depth
380 for reliable small variant calling were obtained, correct star-alleles could be assigned.

381 Furthermore, it was noted that the hybrid was phased to the same allele as all the supposedly false-
382 positive SNVs and INDELs. As the hybrid was not included in the NA12878 reference provided by
383 Krusche *et al.* (34), other variants may also be incorrectly identified in that reference due to the
384 incorrect mapping of the reads originating from the *CYP2D6*-*CYP2D7* hybrid on the *CYP2D6* or *CYP2D7*
385 gene. This can be substantiated with the fact that the reference data set for the NA12878 DNA is mainly

386 constructed based on Illumina short-read sequencing data and older versions of the long-read
387 sequencing technologies, which are more prone to generating inaccurate sequences for complex loci
388 as *CYP2D6-CYP2D7* (42,43). These results indicate that the NA12878 references might be outdated and
389 not entirely accurate, and highlight the advantage of the nCATS enrichment strategy combined with
390 the CoLoRGen pipeline, which can simultaneously detect large structural and small variants.

391 Some other published assays also correctly determine the presence of the *CYP2D6-CYP2D7* *68 allele.
392 However, our nCATS-CoLoRGen assay has added value by providing the complete allele sequences
393 spanning the entire *CYP2D6-CYP2D7* locus, including the exact structural variant sequence. None of
394 the reported assays provide this comprehensive information to the best of our knowledge. LR-PCR
395 could be used as an alternative enrichment strategy, but is mostly only able to target *CYP2D6* (20).
396 Larger regions, including *CYP2D6*, *CYP2D7*, and possible deletions, duplications, and hybrids, are
397 difficult to cover with LR-PCR since the probability of getting chimeric molecules increases with the
398 length of a PCR amplicon (23). TaqMan genotyping combined with quantitative multiplex PCR and LR-
399 PCR validation, or short-read sequencing combined with the statistical modeling and counting Cyrius
400 tool are genotyping approaches that could detect the presence of the *68 hybrid (15,41). Nevertheless,
401 these assays also do not directly provide the allele-specific sequence of the locus, but are instead used
402 to classify the *CYP2D6* locus into a predefined set of star-alleles. However, the current classification of
403 *CYP2D6* enzyme activities based on the star-allele gene definitions has proven to be a suboptimal
404 predictor for enzyme activity (44). More recent research by Van der Lee *et al.* (45) supported this by
405 confirming that building a predictive model based on the complete *CYP2D6* gene sequence gives better
406 predictive values for the gene function than a model built solely based on the star-alleles. By
407 generating complete consensus sequence, CoLoRGen can phase additional mutations, thereby
408 allowing a more accurate gene function predictions.

409 Validation of genotyping performance using two additional cell lines

410 The DNA of two additional cell lines, HG01190 and GM19785, was used to verify the structural variant
411 detection performance of the nCATS-CoLoRGen pipeline. The HG01190 cell line contains two major
412 structural variants (15). One allele has a complete deletion of the *CYP2D6* gene, referred to as the *5
413 allele. The other, *4+*68 allele, contains a duplication, defined as a hybrid between *CYP2D7* and
414 *CYP2D6* (Figure 4). The HG_{combined} dataset contained 37 reads that covered the breakpoints of the
415 12,152 basepair-long deletion between positions 42,123,191 and 42,135,343 (Figure S3). Additionally,
416 a 13,680 basepair-long duplication of the region between positions 42,145,873 and 42,132,193 was
417 discovered in six reads. As more than three reads were covering the breakpoints of the large structural
418 variants, the deletion and insertion were considered to be detected correctly. Subsequently, detection
419 of the small variants was used to exactly identify *CYP2D6*, *CYP2D7*, or possible hybrids. The minimum
420 16X depth for reliable small variant calling was obtained on all detected gene copies except on the
421 insertion of allele 2. Nevertheless, the cell line was correctly identified as the *5/*4+*68 genotype by
422 our CoLoRGen pipeline (Figure 4).

423 The GM19785 cell line consists of a *1 allele, without any structural variants, and a *2+*13 allele,
424 containing one *CYP2D6* copy and a *CYP2D6*-*CYP2D7* hybrid (Figure 4) (15). The hybrid replaces the
425 *CYP2D7* gene in this allele, which implies that there is no difference in the number of gene copies, but
426 only a difference in the DNA sequence on the exact position where *CYP2D7* is normally located.
427 However, the *CYP2D6*-*CYP2D7* hybrid can map on *CYP2D7* due to their highly similar sequences.
428 Therefore, the CoLoRGen pipeline can only detect this structural variant based on the small variants in
429 the gene sequence, and not based on mapped reads with clipping ends. Although insufficient target
430 depths below 16X were reached on both alleles of the GM_{combined} dataset, our CoLoRGen pipeline could
431 assign the correct *1/*2+*13 genotype to the GM19785 DNA (Figure 4).

432 The exact sequence between the *CYP2D6* gene and the *CYP2D6*-*CYP2D7* hybrid could not be
433 determined for the GM19875 cell line, as no reads covering the whole target region were generated.

434 This is due to the presence of a part of the *CYP2D6* sequence at the start of the *CYP2D6-CYP2D7* hybrid,
435 which introduced an additional recognition site for gRNA2 that is normally only present upstream of
436 the *CYP2D6* gene locus. The additional recognition site was visible in the mapped reads, as all the reads
437 were cut in the middle at the same cleavage site (Figure S4). This problem might arise when hybrids
438 are present in the target sequence, but can be circumvented by designing gRNAs located further away
439 from the target gene. However, the further a gRNA is located from the target, the lower the obtained
440 on-target depth will be. This is a trade-off that should be taken into account when designing optimal
441 gRNAs.

442 [In-depth discussion of the generated consensus sequences](#)

443 Although the CoLoRGen pipeline could assign the correct star-alleles to the studied samples, a further
444 in-depth analysis revealed the presence of additional small variants in the final consensus sequences,
445 besides the variants that were assigned to a specific star-allele. Most of these additional variants are
446 present in several sub-allele definitions, thereby confirming the correct assignment of the star-allele.
447 Nevertheless, some additional or lacking variants were often observed in our data compared to the
448 exact sub-allele definition. In the *4 allele of the NA_{combined} and HG_{combined} libraries, 12 additional
449 variants were detected, which were exactly the same for both samples. These variants are all included
450 in several defined sub-alleles, but these sub-alleles contain other variants in addition. In the *1 allele
451 of the GM_{combined} data, two additional deletions were called. One of them was situated in an intron,
452 and the other in an exon region. Both additional deletions were located in homopolymeric regions.
453 The *2 allele of the GM_{combined} data contained 13 additional variants denoted in several *2 sub-allele
454 definitions. Two other additional variants in our data are not defined in the star- or sub-allele database
455 (5) and were both located in exon regions. One of these variants was located in a homopolymeric
456 region. The other variant was not located in a homopolymeric region but represents a synonymous
457 mutation. Therefore, it does not impact the resulting amino acid sequence (Figure S5).

458 The four additionally detected variants that were not present in the star- or sub-allele definitions were
459 all from the GM_{combined} dataset, which had insufficient depths for reliable small variant calling (Figure
460 4). Moreover, three out of these four variants were INDELs located in homopolymeric regions, which
461 are notoriously error-prone regions in ONT sequencing. Therefore, these additionally called variants
462 are probably due to nanopore sequencing errors. The R10.3 flow cell, which has a better performance
463 in homopolymeric regions, was available at the time of writing and is supposed to overcome this
464 problem. However, we decided not to sequence this library on an R10.3 flow cell, as more random
465 errors seem to occur when using this type of flow cell, and R9.4 flow cells still prove to provide better
466 genotyping results (46,47). Nevertheless, efforts are still made by ONT to improve the consensus
467 accuracy of homopolymer regions, which holds promising perspectives for obtaining better results in
468 the future. Another possible explanation for the additional detected variants can be found in the star-
469 allele nomenclature itself. These definitions are intrinsically not comprehensive, as only variants based
470 on microarrays and known effects on the enzyme level are considered in their definitions. Non-coding
471 variants were only considered for recently added star alleles (6). Even though this nomenclature is not
472 optimal in our context of defining complete alleles, the star-allele definitions were used to benchmark
473 our results as no other definitions were yet available at the time of writing. However, a new and more
474 comprehensive system to document gene sequences in the pharmacogenetic field should be a general
475 objective for the future, as the current nomenclature is somewhat outdated.

476 [Variant calling performance of CoLoRGen pipeline versus state-of-the-art variant callers](#)
477 To determine the added value of the newly developed CoLoRGen pipeline, a comparison was made
478 with state-of-the-art variant callers. However, existing small variant detection tools cannot detect large
479 structural variants, and, accordingly, large structural variant detection tools cannot detect small
480 variants. Therefore, separate comparisons were made for the detection of small SNVs and INDELs on
481 the one hand, and large structural variants on the other hand.

482 First, the NA_{combined} dataset was analyzed with the Medaka Variant pipeline to compare the SNV and
483 INDEL calling performance of the CoLoRGen pipeline with the state-of-the-art small variant caller for
484 nanopore sequencing data (31). Although CoLoRGen did not call all SNVs and INDELs correctly, the
485 results were comparable with the results generated by the Medaka Variant pipeline (Table S2). The
486 called SNVs and INDELs that differed between both variant callers were either located in a
487 homopolymeric region or in a region where CoLoRGen detected a hybrid insertion. Homopolymeric
488 regions are a known cause for nanopore sequencing errors and are therefore likely to be responsible
489 for the generation of false-positive small variants (48). Furthermore, regions containing large structural
490 variants, such as hybrid insertions, cannot be detected by the Medaka Variant pipeline. Consequently,
491 reads originating from the hybrid are incorrectly mapped on *CYP2D6* or *CYP2D7* when using the
492 Medaka Variant pipeline, giving rise to more called SNVs and INDELs. However, as the small differences
493 in results between both pipelines can be explained by these two causes, our CoLoRGen pipeline proved
494 to perform adequately for calling SNVs and INDELs in complex genes such as *CYP2D6*. Moreover, as
495 the CoLoRGen pipeline combines both large structural and small variant calling, it can generate a more
496 comprehensive genotype in comparison with the Medaka Variant pipeline.

497 Second, the NA_{combined}, HG_{combined}, and GM_{combined} datasets were also analyzed with the existing large
498 structural variant detection tools NanoVar (30), Sniffles (29), and SVIM (28) to compare the large
499 structural variant calling performance. None of these tools was able to reliably elucidate all the large
500 structural variants in the complex *CYP2D6*-*CYP2D7* locus of the cell lines used in this study (Table S3).
501 Additionally, the output of these tools is not easily interpreted. Therefore, the CoLoRGen tool
502 outperformed these tools as well in terms of generating a correct and comprehensive genotype of the
503 complex *CYP2D6*-*CYP2D7* locus. When aiming for a suitable pharmacogenetic assay to use in clinical
504 practice in the future, a comprehensive and straightforward data analysis tool is of major importance,
505 hence the usefulness of this developed comprehensive CoLoRGen pipeline.

506 [Conclusion](#)

507 In this study, the enrichment efficiencies of the nCATS and the nCATS-AS strategies were assessed on
508 the *CYP2D6-CYP2D7* locus in aiming to develop an assay that can accurately genotype complex
509 pharmacogenes. In addition, we developed and evaluated CoLoRGen, a new and more comprehensive
510 analysis pipeline to simultaneously detect both large structural and small variants. The nCATS-
511 CoLoRGen assay resulted in the assignment of correct star-alleles to the *CYP2D6* gene and *CYP2D6-*
512 *CYP2D7* hybrid in 3 cell lines containing complex gene structures. Moreover, the CoLoRGen pipeline
513 also generated a complete consensus sequence of the genes, thereby demonstrating the presence of
514 *CYP2D6-CYP2D7* large structural variants and smaller SNVs and INDELs that go undetected by other
515 current methods. Our results provide direct evidence that the *CYP2D6* genotype of the NA12878 DNA
516 should include the *CYP2D6-CYP2D7* *68 hybrid and several additional SNVs compared to existing
517 references (15,16,34). However, the implementation of this assay in practice is hampered by the fact
518 that both the nCATS and nCATS-AS strategies led to a low percentage of on-target reads, resulting in
519 low on-target sequencing depths. Further optimization of the nCATS enrichment strategy is thus worth
520 considering for following research, as the usefulness of a long-read PCR-free enrichment strategy in
521 combination with the CoLoRGen pipeline for accurate gene function predictions has been
522 demonstrated in this study.

523 [Availability of data and materials](#)

524 The datasets generated and analyzed during the current study are available as BioProject,
525 PRJNA796180

526 The CoLoRGen pipeline and other used code are available at GitHub:
527 <https://github.com/laurentijntilleman/CoLoRGen>

528 [Competing interests](#)

529 The authors declare that they have no competing interests

530 [Funding](#)

531 KD and this research are supported by the Special Research
532 Fund (Bijzonder Onderzoeksfonds, BOF, University Ghent, BOF21/DOC/042)

533 [Authors' contributions](#)

534 KR: Conceptualization, Methodology, Investigation, Writing – Original Draft, Visualization; LT:
535 Conceptualization, Methodology, Software, Formal Analysis, Investigation, Data Curation, Writing –
536 Original Draft, Visualization; KD: Investigation, Writing – Review & Editing; OT: Methodology, Writing
537 – Review & Editing; DD: Writing – Review & Editing, Funding Acquisition; FV: Conceptualization,
538 Methodology, Writing – Review & Editing, Supervision, Funding Acquisition

539 References

540 1. Evans WE, Relling M V. Moving towards individualized medicine with pharmacogenomics.
541 Nature. 2004 May 27;429(6990):464–8.

542 2. Guo C, Xie X, Li J, Huang L, Chen S, Li X, et al. Pharmacogenomics guidelines: Current status and
543 future development. Clin Exp Pharmacol Physiol. 2019 Aug 16;46(8):689–93.

544 3. Mulder TAM, de With M, del Re M, Danesi R, Mathijssen RHJ, van Schaik RHN. Clinical CYP2D6
545 Genotyping to Personalize Adjuvant Tamoxifen Treatment in ER-Positive Breast Cancer
546 Patients: Current Status of a Controversy. Cancers (Basel). 2021 Feb 12;13(4):771.

547 4. Ingelman-Sundberg M. Pharmacogenetics of cytochrome P450 and its applications in drug
548 therapy: the past, present and future. Trends Pharmacol Sci. 2004 Apr 1;25(4):193–200.

549 5. PharmVar [Internet]. [cited 2021 Jun 4]. Available from:
550 <https://www.pharmvar.org/gene/CYP2D6>

551 6. Nofziger C, Turner AJ, Sangkuhl K, Whirl-Carrillo M, Agúndez JAG, Black JL, et al. PharmVar
552 GeneFocus: CYP2D6. Clin Pharmacol Ther. 2020 Jan 9;107(1):154–70.

553 7. Yang Y, Botton MR, Scott ER, Scott SA. Sequencing the CYP2D6 gene: From variant allele
554 discovery to clinical pharmacogenetic testing. Pharmacogenomics. 2017 May 1;18(7):673–85.

555 8. Nofziger C, Paulmichl M. Accurately genotyping CYP2D6: not for the faint of heart.
556 Pharmacogenomics. 2018 Aug 1;19(13):999–1002.

557 9. Rebsamen MC, Desmeules J, Daali Y, Chiappe A, Diemand A, Rey C, et al. The AmpliChip CYP450
558 test: cytochrome P450 2D6 genotype assessment and phenotype prediction.
559 Pharmacogenomics J 2009 91. 2008 Jul;9(1):34–41.

560 10. Chua EW, Cree SL, Ton KNT, Lehnert K, Shepherd P, Helsby N, et al. Cross-comparison of exome
561 analysis, next-generation sequencing of amplicons, and the iPLEX® ADME PGx panel for

562 pharmacogenomic profiling. *Front Pharmacol.* 2016;7.

563 11. Gaedigk A, Riffel AK, Leeder JS. CYP2D6 Haplotype Determination Using Long Range Allele-
564 Specific Amplification: Resolution of a Complex Genotype and a Discordant Genotype Involving
565 the CYP2D6*59 Allele. *J Mol Diagn.* 2015 Nov;17(6):740.

566 12. Everts RE, Ph D, Metzler H, D VHP, D CHP, Nunez R. Development and Research Validation of
567 the iPLEX® ADME PGx Panel on the MassARRAY® System. *Biotech Protoc Guid.* 2012;2–6.

568 13. Tillemans L, Weymaere J, Heindryckx B, Deforce D, Nieuwerburgh F Van. Contemporary
569 pharmacogenetic assays in view of the PharmGKB database. *Pharmacogenomics.* 2019 Mar
570 1;20(4):261–72.

571 14. Arbitrio M, Martino MT Di, Scionti F, Agapito G, Guzzi PH, Cannataro M, et al. DMET TM (Drug
572 Metabolism Enzymes and Transporters): a pharmacogenomic platform for precision medicine.
573 *Oncotarget.* 2016 Jun 9;7(33):54028–50.

574 15. Gaedigk A, Turner A, Everts RE, Scott SA, Aggarwal P, Broeckel U, et al. Characterization of
575 Reference Materials for Genetic Testing of CYP2D6 Alleles: A GeT-RM Collaborative Project. *J
576 Mol Diagnostics.* 2019 Nov 1;21(6):1034–52.

577 16. Pratt VM, Everts RE, Aggarwal P, Beyer BN, Broeckel U, Epstein-Baak R, et al. Characterization
578 of 137 Genomic DNA Reference Materials for 28 Pharmacogenetic Genes: A GeT-RM
579 Collaborative Project. *J Mol Diagnostics.* 2016 Jan 1;18(1):109–23.

580 17. Clinical Annotations [Internet]. [cited 2022 Jan 7]. Available from:
581 <https://www.pharmgkb.org/clinicalAnnotations>

582 18. Ammar R, Paton TA, Torti D, Shlien A, Bader GD. Long read nanopore sequencing for detection
583 of HLA and CYP2D6 variants and haplotypes. *F1000Research.* 2015 May 20;4:17.

584 19. Fukunaga K, Hishinuma E, Hiratsuka M, Kato K, Okusaka T, Saito T, et al. Determination of novel

585 CYP2D6 haplotype using the targeted sequencing followed by the long-read sequencing and the
586 functional characterization in the Japanese population. *J Hum Genet.* 2021 Feb 5;66(2):139–49.

587 20. Liau Y, Maggo S, Miller AL, Pearson JF, Kennedy MA, Cree SL. Nanopore sequencing of the
588 pharmacogene CYP2D6 allows simultaneous haplotyping and detection of duplications.
589 *Pharmacogenomics.* 2019 Sep 27;20(14):1033–47.

590 21. Qiao W, Yang Y, Sebra R, Mendiratta G, Gaedigk A, Desnick RJ, et al. Long-Read Single Molecule
591 Real-Time Full Gene Sequencing of Cytochrome P450-2D6. *Hum Mutat.* 2016 Mar;37(3):315–
592 23.

593 22. Buermans HPJ, Vossen RHAM, Anvar SY, Allard WG, Guchelaar HJ, White SJ, et al. Flexible and
594 Scalable Full-Length CYP2D6 Long Amplicon PacBio Sequencing. *Hum Mutat.* 2017 Mar
595 1;38(3):310–6.

596 23. Laver TW, Caswell RC, Moore KA, Poschmann J, Johnson MB, Owens MM, et al. Pitfalls of
597 haplotype phasing from amplicon-based long-read sequencing. *Sci Rep.* 2016 Feb 17;6(1):1–6.

598 24. Gilpatrick T, Lee I, Graham JE, Raimondeau E, Bowen R, Heron A, et al. Targeted nanopore
599 sequencing with Cas9-guided adapter ligation. *Nat Biotechnol.* 2020 Apr 1;38(4):433–8.

600 25. López-Girona E, Davy MW, Albert NW, Hilario E, Smart MEM, Kirk C, et al. CRISPR-Cas9
601 enrichment and long read sequencing for fine mapping in plants. *Plant Methods.* 2020 Sep
602 1;16(1):1–13.

603 26. Community - Info sheet - Targeted, amplification-free DNA sequencing using CRISPR/Cas
604 [Internet]. [cited 2021 Jun 10]. Available from:
605 https://community.nanoporetech.com/info_sheets/targeted-amplification-free-dna-sequencing-using-crispr-cas/v/eci_s1014_v1_reve_11dec2018

607 27. Loose M, Malla S, Stout M. Real-time selective sequencing using nanopore technology. *Nat
608 Methods.* 2016 Aug 30;13(9):751–4.

609 28. Heller D, Vingron M. SVIM: structural variant identification using mapped long reads.
610 Bioinformatics. 2019 Sep 1;35(17):2907–15.

611 29. Sedlazeck FJ, Rescheneder P, Smolka M, Fang H, Nattestad M, von Haeseler A, et al. Accurate
612 detection of complex structural variations using single-molecule sequencing. Nat Methods.
613 2018 Jun 30;15(6):461–8.

614 30. Tham CY, Tirado-Magallanes R, Goh Y, Fullwood MJ, Koh BTH, Wang W, et al. NanoVar: accurate
615 characterization of patients' genomic structural variants using low-depth nanopore sequencing.
616 Genome Biol. 2020 Dec 3;21(1):56.

617 31. GitHub - nanoporetech/medaka: Sequence correction provided by ONT Research [Internet].
618 [cited 2021 Dec 15]. Available from: <https://github.com/nanoporetech/medaka>

619 32. Labun K, Montague TG, Krause M, Torres Cleuren YN, Tjeldnes H, Valen E. CHOPCHOP v3:
620 expanding the CRISPR web toolbox beyond genome editing. Nucleic Acids Res. 2019 Jul
621 2;47(W1):W171–4.

622 33. Nofziger C, Turner AJ, Sangkuhl K, Whirl-Carrillo M, Agúndez JAG, Black JL, et al. PharmVar
623 GeneFocus: CYP2D6. Clin Pharmacol Ther. 2020;107(1):154–70.

624 34. Krusche P, Trigg L, Boutros PC, Mason CE, De La Vega FM, Moore BL, et al. Best practices for
625 benchmarking germline small-variant calls in human genomes. Nat Biotechnol. 2019;37(5):555–
626 60.

627 35. GitHub - Illumina/hap.py: Haplotype VCF comparison tools [Internet]. [cited 2021 Oct 27].
628 Available from: <https://github.com/Illumina/hap.py>

629 36. laurentijntillemans/visualize_CoLoRGen: Extra scripts for visualizing CoLoRGen output
630 [Internet]. [cited 2022 Mar 30]. Available from:
631 https://github.com/laurentijntillemans/visualize_CoLoRGen

632 37. GitHub - lh3/seqtk: Toolkit for processing sequences in FASTA/Q formats [Internet]. [cited 2021
633 Oct 27]. Available from: <https://github.com/lh3/seqtk>

634 38. laurentijntilleman/CoLoRGen: CoLoRGen: comprehensive long read genotyping pipeline.
635 [Internet]. [cited 2022 Mar 30]. Available from:
636 <https://github.com/laurentijntilleman/CoLoRGen>

637 39. Payne A, Holmes N, Clarke T, Munro R, Debebe BJ, Loose M. Readfish enables targeted
638 nanopore sequencing of gigabase-sized genomes. *Nat Biotechnol.* 2021 Apr 1;39(4):442–50.

639 40. Community - Protocol - Cas9 targeted sequencing [Internet]. [cited 2021 Oct 26]. Available
640 from: https://community.nanoporetech.com/protocols/cas9-targeted-sequencing/v/enr_9084_v109_revs_04dec2018

642 41. Chen X, Shen F, Gonzaludo N, Malhotra A, Rogert C, Taft RJ, et al. Cyrius: accurate CYP2D6
643 genotyping using whole-genome sequencing data. *Pharmacogenomics J.* 2021 Apr 1;21(2):251–
644 61.

645 42. Zook JM, Catoe D, McDaniel J, Vang L, Spies N, Sidow A, et al. Extensive sequencing of seven
646 human genomes to characterize benchmark reference materials. *Sci Data.* 2016 Dec 7;3(1):1–
647 26.

648 43. Eberle MA, Fritzilas E, Krusche P, Källberg M, Moore BL, Bekritsky MA, et al. A reference data
649 set of 5.4 million phased human variants validated by genetic inheritance from sequencing a
650 three-generation 17-member pedigree. *Genome Res.* 2017 Jan 1;27(1):157–64.

651 44. Hicks J, Swen J, Gaedigk A. Challenges in CYP2D6 Phenotype Assignment from Genotype Data:
652 A Critical Assessment and Call for Standardization. *Curr Drug Metab.* 2014 Mar 29;15(2):218–
653 32.

654 45. Van der Lee M, Allard WG, Vossen RHAM, Baak-Pablo RF, Menafra R, Deiman BALM, et al.
655 Toward predicting CYP2D6-mediated variable drug response from CYP2D6 gene sequencing

656 data. *Sci Transl Med.* 2021 Jul 21;13(603):3637.

657 46. González-Recio O, Gutiérrez-Rivas M, Peiró-Pastor R, Aguilera-Sepúlveda P, Cano-Gómez C,
658 Ángel Jiménez-Clavero M, et al. Sequencing of SARS-CoV-2 genome using different nanopore
659 chemistries. *Appl Genet Mol Biotechnol.*

660 47. Tytgat O, Škevin S, Deforce D, Van Nieuwerburgh F. Nanopore sequencing of a forensic
661 combined STR and SNP multiplex. *Forensic Sci Int Genet.* 2022 Jan;56:102621.

662 48. Delahaye C, Nicolas J. Sequencing DNA with nanopores: Troubles and biases. *PLoS One.* 2021
663 Oct 1;16(10):e0257521.

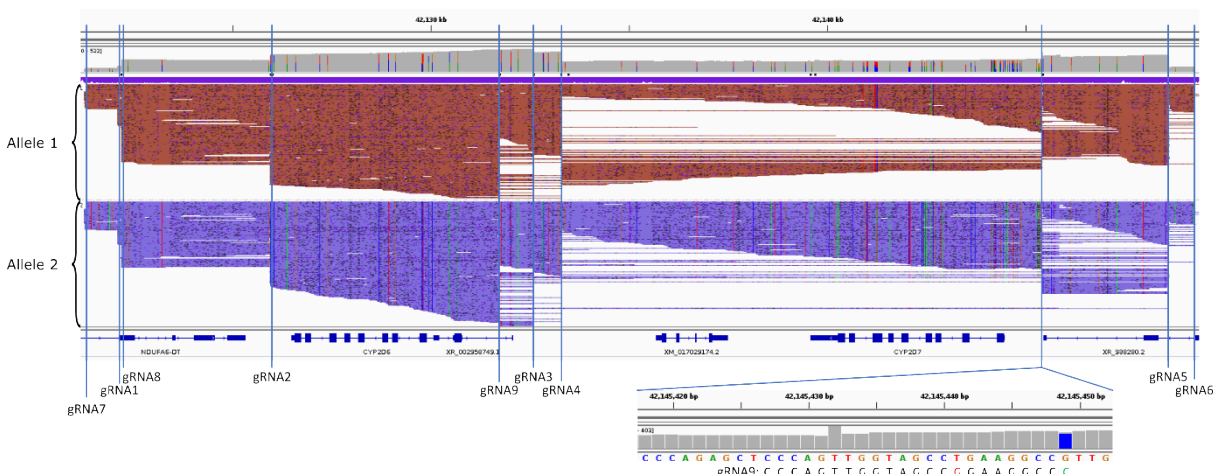
665 Supplemental material: Cas9 targeted

666 nanopore sequencing with enhanced

667 variant calling improves *CYP2D6-CYP2D7*

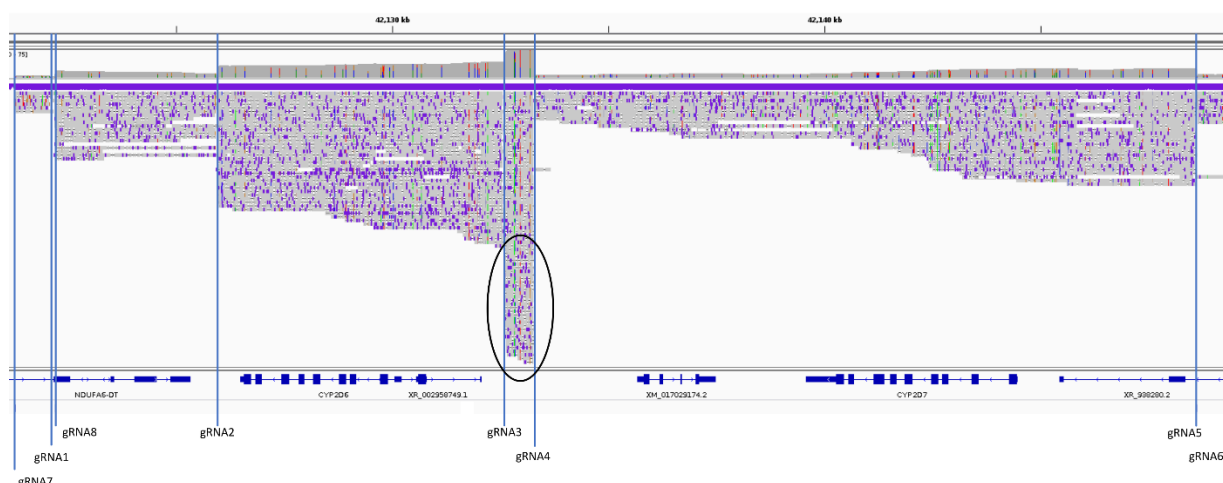
668 hybrid allele genotyping

669 **Figures**



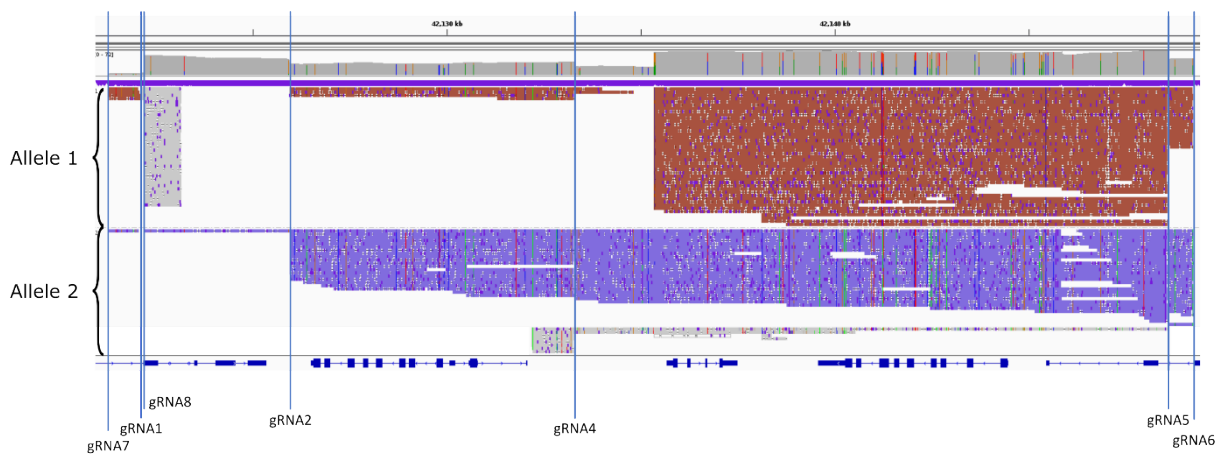
670

671 *Figure S1* Mapped reads of the NA12878 DNA sequenced on a MinION flow cell. The positions of the gRNAs are indicated
672 with vertical lines. Reads are split by allele. The position where gRNA9 binds off-target is zoomed in. This recognition site
673 shows one mismatch (red) and one mutation (green).



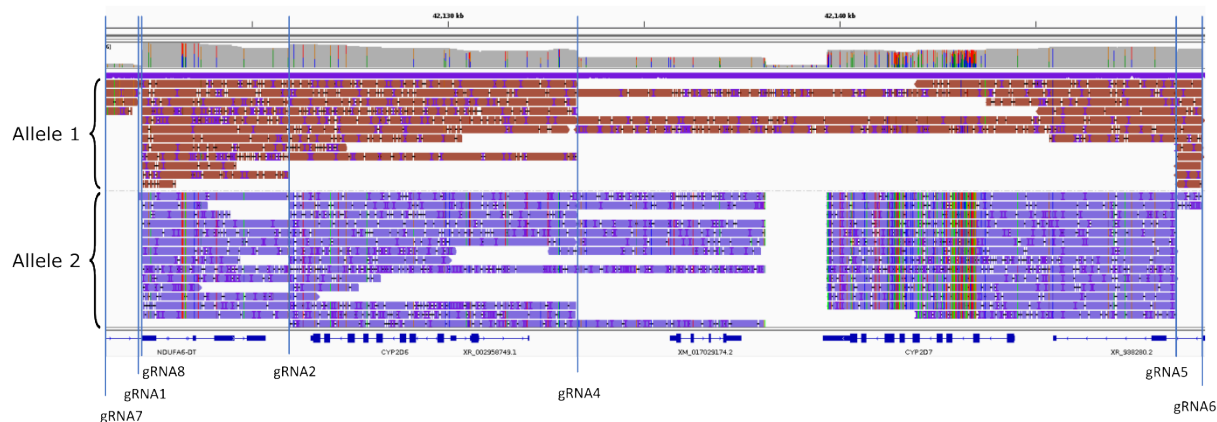
674

675 *Figure S2* Mapped reads of the NA12878 DNA sequenced on a Flongle flow cell. The positions of the gRNAs are indicated with
676 vertical lines. gRNA3 cut reads generated by gRNA4, causing a lower depth on *CYP2D6*.

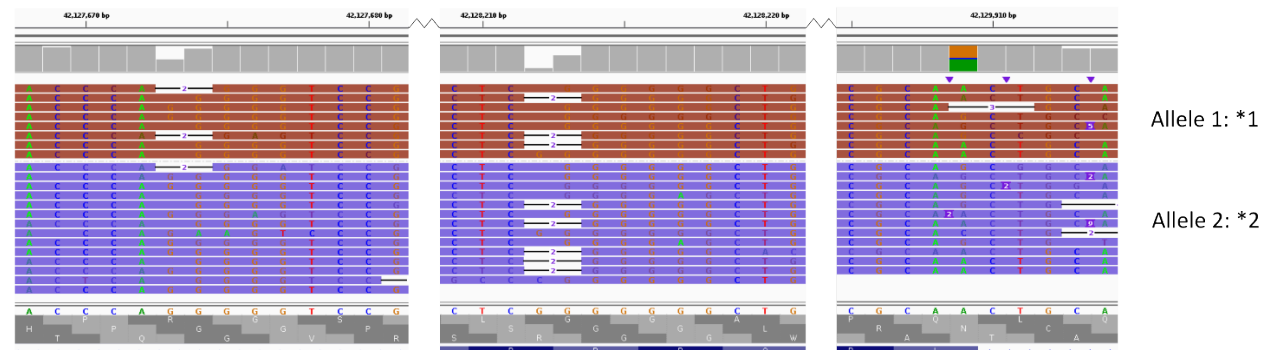


677

678 *Figure S3* Mapped reads of the HG01190 DNA sequenced on a MinION flow cell. The HG_{combined} dataset was used to generate
679 this figure, which is the dataset containing both the positively selected reads from the AS pores and all the reads from the
680 conventionally sequencing pores. The positions of the gRNAs are indicated with vertical lines. Reads are split by allele, and
681 gray reads are clipping ends that were cut in-silico and mapped separately.



683 *Figure S4* Mapped reads of the GM19785 DNA sequenced on a MinION flow cell. The GM_{combined} dataset was used to generate
684 this figure, which is the dataset containing both the positively selected reads from the AS pores and all the reads from the
685 conventionally sequencing pores. The positions of the gRNAs are indicated with vertical lines. Reads are split by allele.



687 *Figure S5* CoLoRGen detected four additional small variants in the GM19785 cell line that are not present in the sub-allele
688 definitions. The three deletions were located in homopolymeric regions and the SNV is a silent mutation.

689 Tables

690 *Table S1* Overview of the used guide RNAs (gRNAs).

Guide RNA	Sequence	PAM
gRNA1	CCATTCAACCCTTATGCTCAG	GGG
gRNA2	AGTCCTGTGGTGAGGTGACG	AGG
gRNA3	GCCATACAATCCACCTGTAG	AGG
gRNA4	CTTCCGACATACACGCAAT	GGG
gRNA5	TTCCCCACTTTTACTACAC	AGG
gRNA6	CAAAGTCCATGCGTAAGTCT	TGG
gRNA7	TCTCACCAAGCAATAACCGAG	AGG
gRNA8	ACCTCCGGTTGCTTCCTGAG	GGG
gRNA9	GGGCCTTCCGGCTACCAACT	GGG

691

692 *Table S2* Comparison of small SNV and INDEL variant detection of the Medaka Variant pipeline and the new CoLoRGen tool

693 in the NA12878 DNA sample. Reference: Krusche *et al.* (34).

Run	Correctly called and phased SNVs (<i>CYP2D6 + CYP2D7</i>)	Incorrectly called SNVs (<i>CYP2D6 + CYP2D7</i>)	Correctly called and phased INDELS (<i>CYP2D6 + CYP2D7</i>)	Incorrectly INDELS (<i>CYP2D6 + CYP2D7</i>)
Reference	11 + 26	/	1 + 1	/
CoLoRGen	11 + 26	2 + 5	1 + 0	0 + 4
Medaka	11 + 26	2 + 6	1 + 1	1 + 3

694

695 Table S3 Comparison of structural variant detection of different state-of-the-art structural variant tools and the new
 696 CoLoRGen tool in the NA12878, HG01190 and GM19785 DNA samples. For each tool the number of deletions and insertions
 697 are given. Between parentheses the length of each variant is given. Green: correctly detected structural variant; red:
 698 incorrectly detected structural variant; orange: multiple overlapping structural variants are detected although only one
 699 variant is present in the reference. Reference: Get-RM studies (15,16). †: the found regions show overlap.

	NA12878		HG01190		GM19785	
	deletion	insertion	deletion	insertion	deletion	insertion
Reference	/	*68	*5	*68	/	/
CoLoRGen	/	1 (13,680 bp)	1 (12,152 bp)	1 (13,680 bp)	/	/
NanoVar (PASS)	/	/	/	1 (13,838 bp)	/	/
Sniffles (PASS)	2 (12,282 bp, 12,152 bp) †	3 (12,154 bp, 13,708 bp, 13,659 bp) †	2 (12,454 bp, 12,155 bp) †	1 (1,006 bp)	1 (13,656 bp)	/
SVIM (QUAL ≥3, PASS)	/	2 (13,638 bp, 13,613 bp) †	/	1 (13,424 bp)	2 (13,696 bp, 13,663 bp) †	/

700

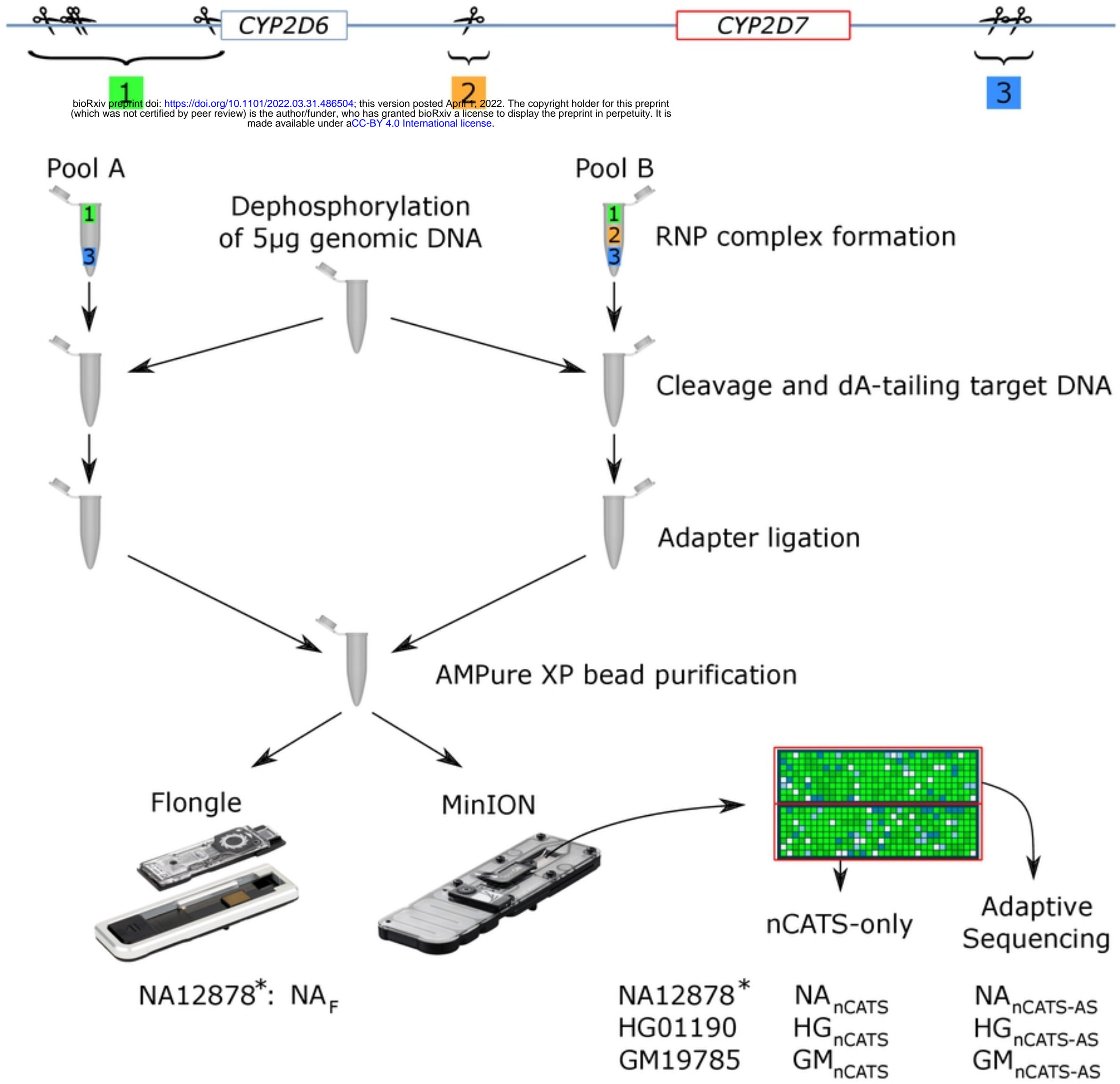
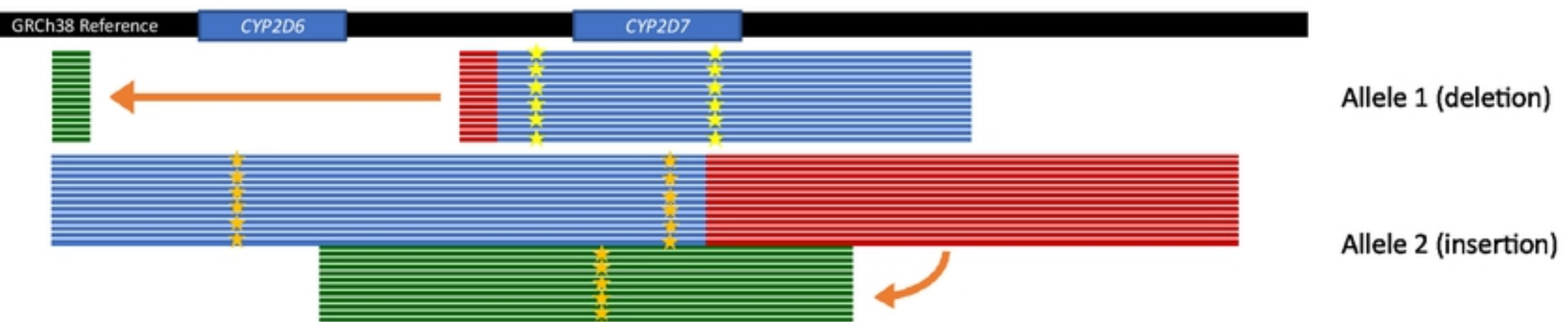
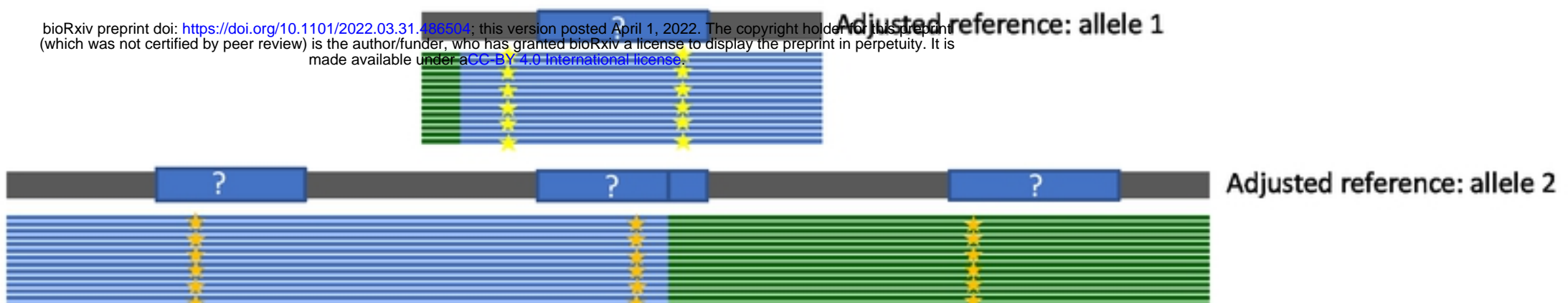


Figure 1

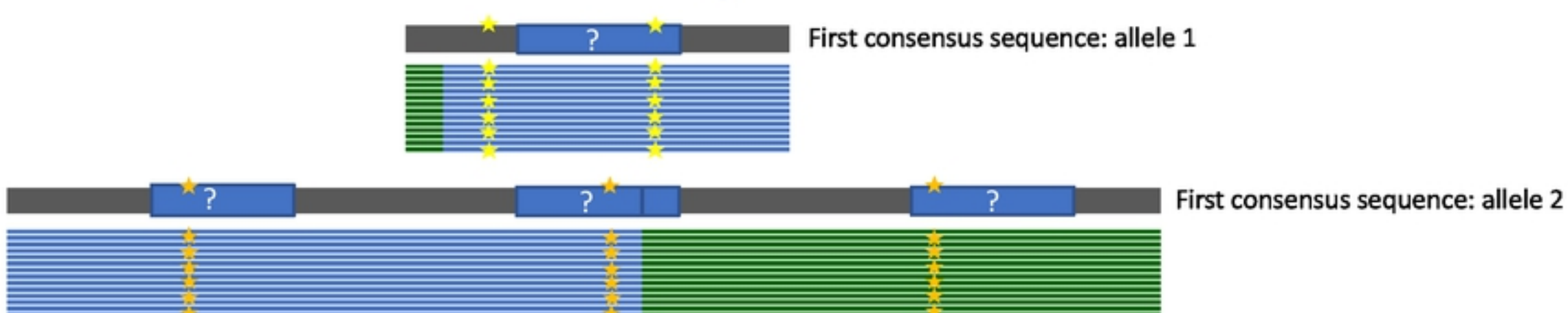
A: Mapping on reference genome (blue), clipping-end detection (red) and remapping (green)



B: Adjustment of the reference based on breakpoints



C: Adjustment of the reference based on small variants



D: Generation of final consensus and determination of the CYP genes and hybrids

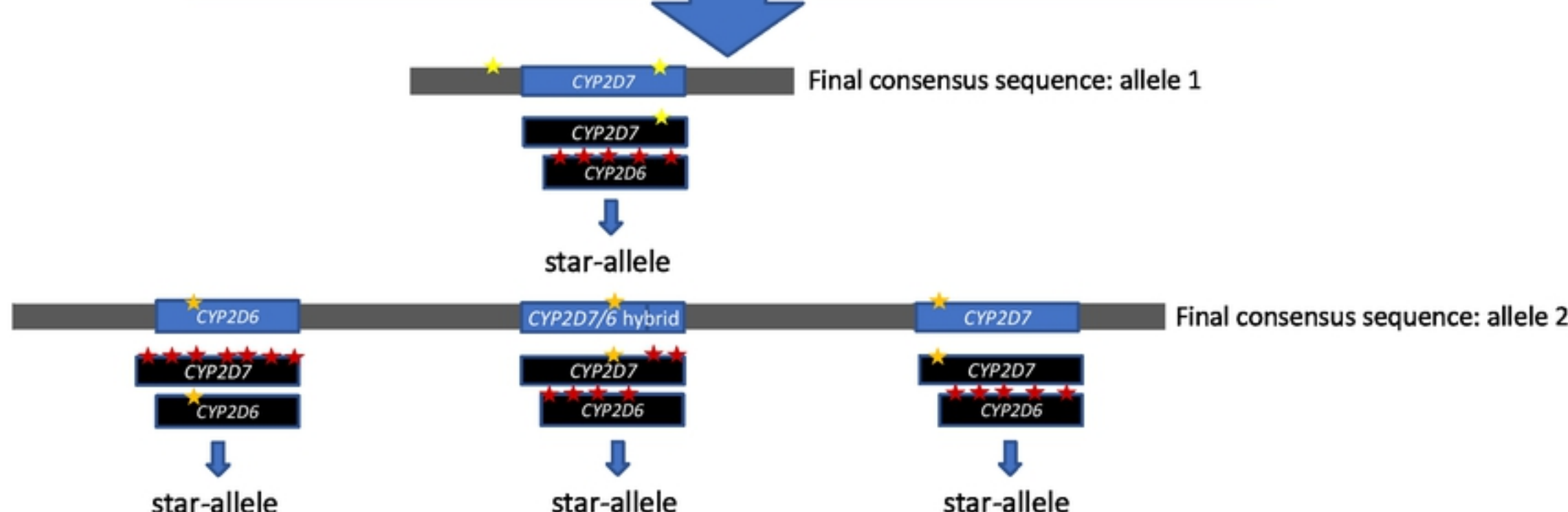
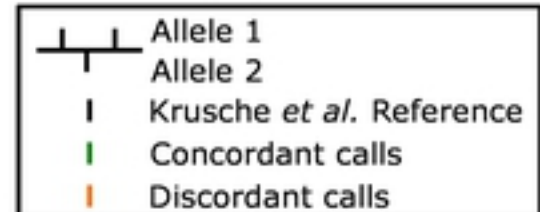
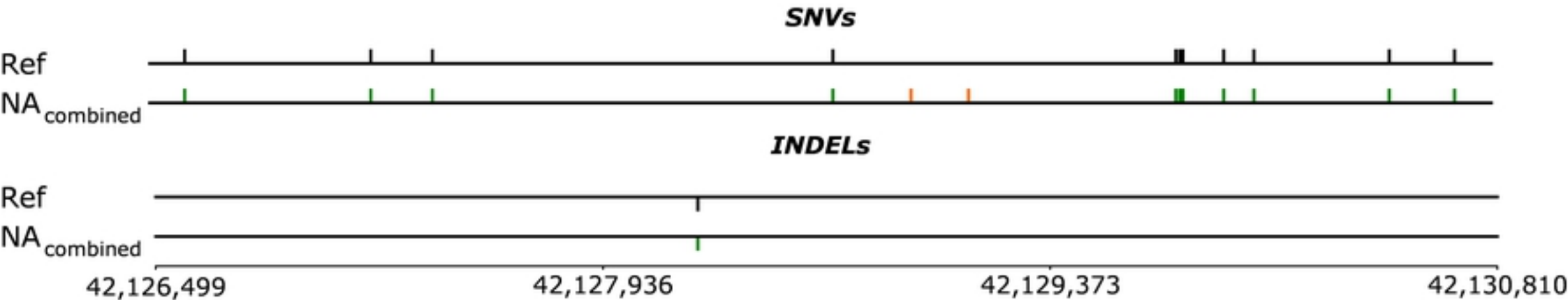


Figure 2



A: CYP2D6



B: CYP2D7

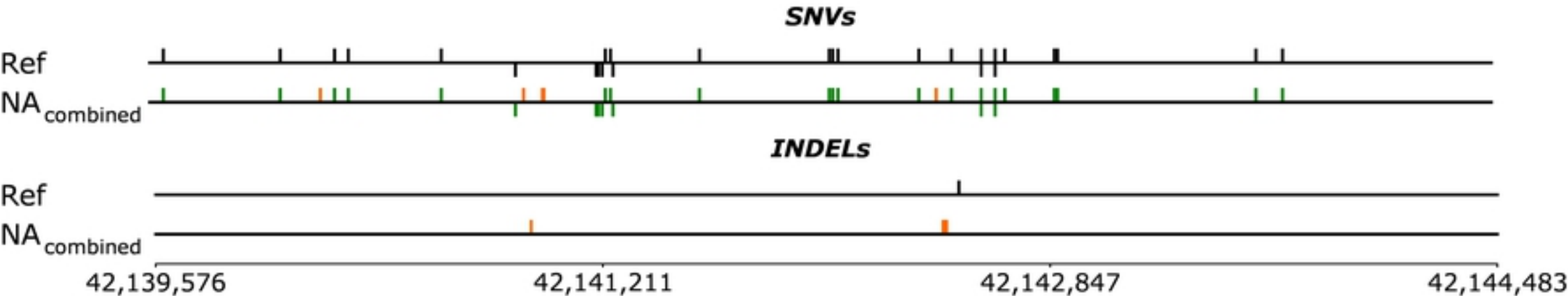


Figure 3

NA12878

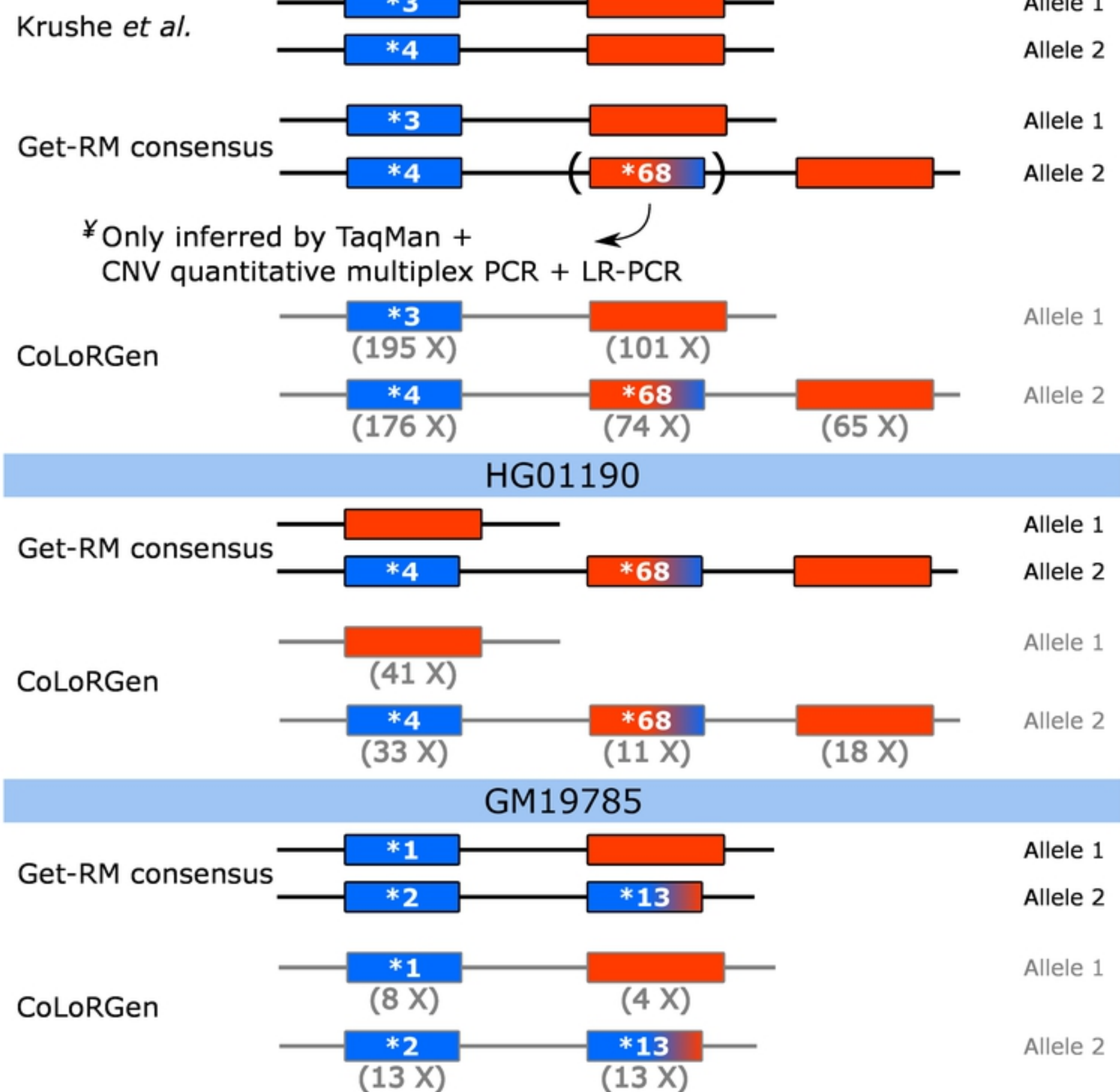
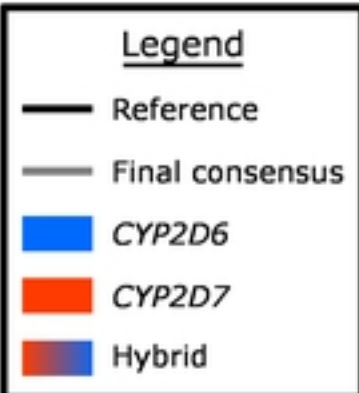


Figure 4